Science of the Total Environment 727 (2020) 138584

Contents lists available at ScienceDirect

Science of the Total Environment

journal homepage: www.elsevier.com/locate/scitotenv

Factors influencing the boundary layer height and their relationship with air quality in the Sichuan Basin, China

Bangjun Cao [a,*], Xiaoyan Wang [b], Guicai Ning [c], Liang Yuan [a], Mengjiao Jiang [a], Xiaoling Zhang [a], Shigong Wang [a]

[a] Plateau Atmosphere and Environment Key Laboratory of Sichuan Province, School of Atmospheric Sciences, Chengdu University of Information Technology, Chengdu 610225, China
[b] Department of Atmospheric and Oceanic Sciences, Institute of Atmospheric Sciences, Fudan University, Shanghai 200438, China
[c] Institute of Environment, Energy and Sustainability, The Chinese University of Hong Kong, Hong Kong 999077, China

HIGHLIGHTS

- Factors affecting the boundary layer height (h_{max}) change in Sichuan Basin.
- The inversion layer in troposphere is the main factor affecting h_{max} on cloudy days.
- The vertical wind shear is the main factors affecting h_{max} on sunny days.
- The secondary circulation is much weaker on cloudy days than on sunny days.

GRAPHICAL ABSTRACT

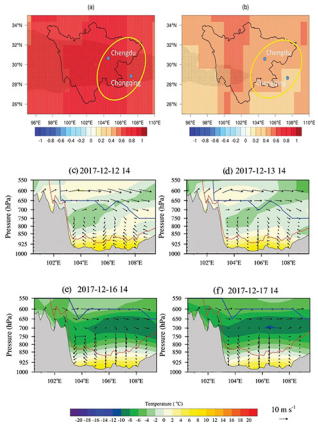

ARTICLE INFO

Article history:
Received 26 October 2019
Received in revised form 7 April 2020
Accepted 7 April 2020
Available online 11 April 2020

Editor: Mandhoolika Agrawal

Keywords:
Air quality
Boundary layer height
Surface sensible heat flux
Wind shear
Sichuan Basin

ABSTRACT

We investigated the factors influencing the daily maximum boundary layer height (h_{max}) and their relationship with air quality in the Sichuan Basin, China. We analyzed the factors influencing h_{max} on cloudy and sunny days in winter using five years of observational data and a reanalysis dataset and investigated the relationship between h_{max} and air quality. The inversion layer in the lower troposphere has a critical impact on h_{max} on cloudy days. By contrast, the sensible heat flux and wind shear are the main influencing factors on sunny days, although the contribution of the sensible heat flux to h_{max} is less than that of the wind shear. This is because the turbulence is mainly affected by mechanical mixing induced by the topographic effect of the Tibetan Plateau to the west of the Sichuan Basin. The secondary circulation over the Sichuan Basin is weaker on cloudy days than on sunny days. These results are important for understanding the dispersion of air pollutants over the Sichuan Basin.

* Corresponding author at: School of Atmospheric Sciences, Chengdu University of Information Technology, No. 24, Block 1, Xuefu Road, Chengdu 610225, China.
E-mail address: caobj1989@163.com (B. Cao).

https://doi.org/10.1016/j.scitotenv.2020.138584
0048-9697/

1. Introduction

The Sichuan Basin is located in the center of the Sichuan–Chongqing region of China, which includes Sichuan Province and Chongqing city. The topography of the Sichuan–Chongqing region is complex. The Tibetan Plateau lies to the west of the Sichuan Basin and the Panxi Plateau lies to the southwest. The climate of this region shows wide variations as a result of this varied topography. The Sichuan Basin is a region of major haze in China due to large anthropogenic emissions and the high population density (J. Li et al., 2016). Various atmospheric pollutants are concentrated in high-intensity emissions and have led to a significant deterioration in the local air quality. Haze, photochemical smog and other types of atmospheric pollution frequently occur over the Sichuan Basin. The air pollution shows clear regional characteristics (Ning et al., 2017) and is affected by the unique topography and climate of the region. The environmental problems caused by the deterioration in air quality cannot be neglected by industry (Cai et al., 2017; Sheehan et al., 2014; Zhang et al., 2014; Zhang and Cao, 2015) because they affect the lifestyle and health of the local population (Pope et al., 2002; Künzli et al., 2005; Cohen et al., 2017). The environmental effects caused by the deterioration in air quality have aroused widespread public concern. The government has implemented strict air pollution control measures in recent years and the air quality improved between 2013 and 2016 in most areas of Sichuan and Chongqing.

The air quality is affected by both the emission sources and the meteorological conditions. Severe air pollution events are related to meteorological conditions with a poor capacity to disperse pollutants, the structure of the planetary boundary layer, particular weather systems and the atmospheric circulation (Bi et al., 2014; Deng et al., 2014; Gu and Yim, 2016; Q. Li et al., 2016; Chen and Wang, 2015; Ye et al., 2016; Zhang et al., 2003; Ning et al., 2018, 2019). Meteorological conditions are the direct reason of dramatic short-term changes in air quality. The characteristics of the atmospheric boundary layer are closely related to the dispersion and transport of pollutants and the boundary layer height (BLH) is an important factor affecting air quality (Liao et al., 2017; Zhang et al., 2016). The BLH varies day by day and compresses the volume in which pollutants can be dispersed. A decrease in the BLH favors the accumulation of air pollutants, which leads to a deterioration in air quality. The diurnal variation of pollutants in the atmospheric boundary layer involves various feedback processes and is related to a number of different factors (Wang et al., 2016).

Many factors affect the thermodynamic and dynamic processes of the atmosphere near the surface. These processes are the source of heat and energy in the convective boundary layer (CBL) (LeMone et al., 2007). Dynamic processes usually refer to wind shear (Moeng and Sullivan, 1994; Huang et al., 2014) and thermal processes refer to the buoyancy generated by heating of the underlying surface. Buoyancy and wind shear are important mechanisms affecting the development of turbulence and the spatio-temporal distribution of physical quantities in the CBL. The air in the CBL is fully mixed by heat bubble convection and wind shear. The effect of the sensible heat flux on the CBL has been confirmed by large eddy simulations (Maronga and Raasch, 2013). Other factors, such as the scale of the heterogeneous surface and the turbulent coherent structure, have a significant impact on the local development and thickness of the CBL. In addition, a neutral residual layer covers the CBL in the desert areas of northwestern China and the decreased surface heat flux determines the growth of the CBL (Han et al., 2015), which varies between regions.

The most notable weather phenomenon in the Sichuan Basin is the deep, strong inversion layer between about 3200 and 4200 m. This is different from the inversion layer in the upper boundary layer, which is at a height of about 1000–2000 m (Ning et al., 2018). This inversion layer acts as a cover and affects the activity of the atmosphere within the atmospheric boundary layer (Ning et al., 2018). The strong inversion layer in the lower troposphere over the Sichuan Basin leads to the accumulation of a large amount of water vapor below the inversion layer. The inversion at the height of the plateau over eastern China is generated by the advection of warm air from the plateau, which provides favorable thermodynamic conditions for mid-level clouds (J. Li et al., 2016). These clouds have a significant effect on the development of the CBL (Jiang et al., 2009).

Previous studies have not taken into account the influence of different factors on the BLH in the Sichuan Basin. When the cloud cover decreases from cloudy days to sunny days in winter, the mid-level clouds disappear and the BLH is not affected by clouds at a height of 2000–4000 m (Jiang et al., 2009). On sunny days the BLH is determined by the intensity of the wind shear (the dynamic factor) and the surface sensible heat flux (the thermal factor) and other, as yet unknown, factors. It is therefore necessary to evaluate which factors determine the growth of the CBL in the Sichuan Basin. This is important in studies of the physical mechanisms of the development of the atmospheric boundary layer. Few studies have explored the effect of the BLH on air quality in the Sichuan Basin. We used observational data and a reanalysis dataset to divide the weather conditions during the winter months into cloudy and sunny days. We then investigated the factors affecting the BLH on cloudy and sunny days and the relationship between the

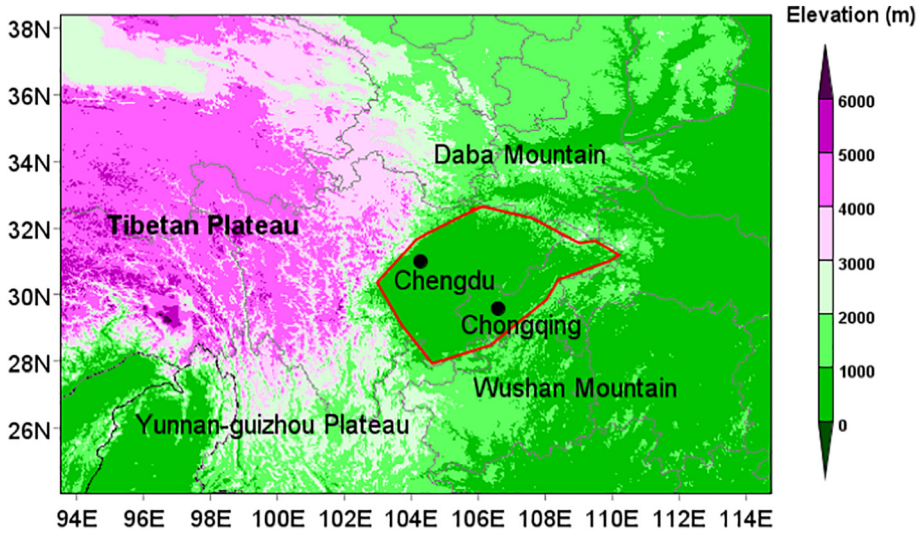

Fig. 1. Topographic map (shading; units: m) of the Sichuan Basin (delineated in red) and surrounding areas showing the location of Chengdu and Chongqing stations (black dots).

Table 1
Root-mean-square errors (RMSE) between the ERA-Interim dataset and the observational data.

RMSE	Pressure level (hPa)				
	900	800	700	600	500
Temperature (°C)	2.1	2.8	2.3	3.2	4.3
Wind speed (m s^{-1})	1.3	1.5	1.5	2.4	3.4
Specific humidity (kg kg^{-1})	2.2	2.6	2.7	3.7	4.2

BLH and air quality. It is very important for understanding the development mechanism of boundary layer and the dispersion of air pollutants under different weather conditions over the Sichuan Basin.

2. Data and methods

2.1. Location of the Sichuan Basin

Sichuan Province is located in southwest China. There are 22 cities in this region, including Chengdu and Chongqing. Sichuan Province is regarded as one of the most topographically complex areas in the world (Liao et al., 2018). There are large differences in topographic height across the region and the province can be divided into three areas: the Sichuan Basin, the western Sichuan Plateau and the Panxi Plateau (Fig. 1). The region has experienced rapid economic development in recent decades and has a high population density.

2.2. Meteorological data

We obtained the temperature, geopotential height, and the u and v components of wind from the ERA-Interim daily dataset to analyze the dynamic and thermodynamic conditions in the boundary layer. The ERA-Interim dataset is a global atmospheric reanalysis dataset from 1979 and is continuously updated in real time. The ERA-Interim dataset includes both analyses (four times per day at 00:00, 06:00, 12:00 and 18:00 h UTC) and forecasts (from 00:00 and 12:00 in steps of 3, 6, 9 and 12 h). The spatial resolution of the dataset is about 80 km (T255 spectral) on 60 vertical levels from the Earth's surface to a height of 0.1 hPa. Surface and single-level field forecasts are available to download from the web site (http://apps.ecmwf.int/datasets/data/interim-full-daily/levtype=pl/). We obtained data for five winters (from December to February of the next year) from December 2014 to February 2019, including December 2014, 2015, 2016, 2017, 2018 and 2019, and January and February 2015, 2016, 2017, 2018, 2019 (named as Y1, Y2, Y3, Y4 and Y5).

The BLH was obtained from the ERA-Interim daily dataset at the surface with a 3 h temporal resolution (00:00, 03:00, 06:00, 09:00, 12:00, 15:00, 18:00 and 21:00 h UTC) (http://apps.ecmwf.int/datasets/data/interim-full-daily/levtype=sfc/). This BLH is the level at which the bulk Richardson number (Ri_{cr}) reaches the key value $Ri_{cr} = 0.25$ (Beljaars, 2006; Troen and Mahrt, 1986). The Ri_{cr} is calculated based on the difference between quantities at that level and the lowest model level. The bulk Richardson is computed from the following set of equations:

$$|\Delta U|^2 = (u_{hbl} - u_n)^2 + (v_{hbl} - v_n)^2 \quad (1)$$

$$s_{vn} = c_p T_n (1 + \varepsilon q_n) + g z_n + 0.5K \quad (2)$$

$$s_{vhbl} = c_p T_{hbl} (1 + \varepsilon q_{hbl}) + g h_{bl} \quad (3)$$

$$\Delta s = 8.5 c_p Q_{0v} / w_s \quad (4)$$

$$w_s = \left\{ u_*^3 + 0.6(g/T) Q_{0v} h_{bl} \right\}^{1/3} \quad unstable \quad (5)$$

$$w_s = u_* \quad stable \quad (6)$$

$$Ri_b = h_{bl} \frac{2g(s_{vhbl} - s_{vn} - \Delta s)}{(s_{vhbl} + s_{vn} - g h_{bl} - g z_n)|\Delta U|^2} \quad (7)$$

where index n indicates the lowest model level and h_{bl} indicates the boundary layer height where the level $Ri_b = Ri_{cr}$. The virtual dry static energy from the lowest level s_{vn} is increased with a turbulent part Δs and compared to the virtual dry static energy at boundary layer height h_{bn}. The boundary layer height is found by a vertical scan from the surface upwards. If the boundary layer height is found to be between two levels a linear interpolation is done to find the exact position. Since the boundary layer height is needed for w_s, the upward scan is done twice. The first one uses $h_{bl} = 1000$ m in the expression for w_s; the second scan uses the result of the first scan.

Measurements from radiosondes launched at Chengdu (30.70° N, 103.83° E; elevation 541.0 m) (Fig. 1) and Chongqing (29.44° N, 106.37° E; elevation 464.7 m) stations at 00:00 and 12:00 h UTC (08:00 and 20:00 h local time) were obtained from the University of Wyoming website (http://weather.uwyo.edu/upperair/sounding.html) and included the temperature, potential temperature and horizontal wind profiles. Chengdu and Chongqing meteorological stations

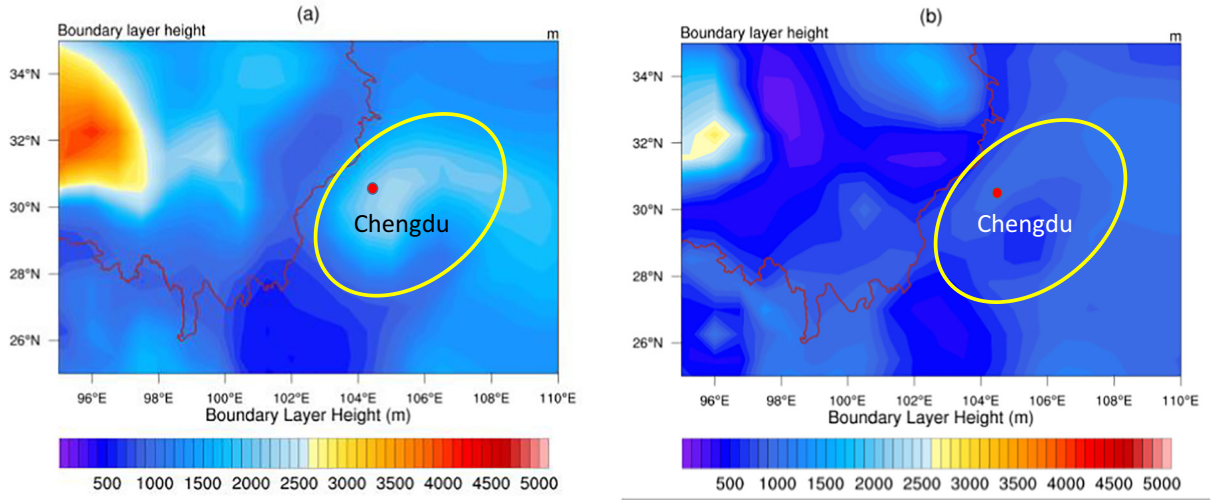

Fig. 2. Distribution of the boundary layer height in the Sichuan Basin on (a) sunny and (b) cloudy days in winter 2014–2019. The oval outline is the Sichuan Basin and the red line is the border of the Tibetan Plateau.

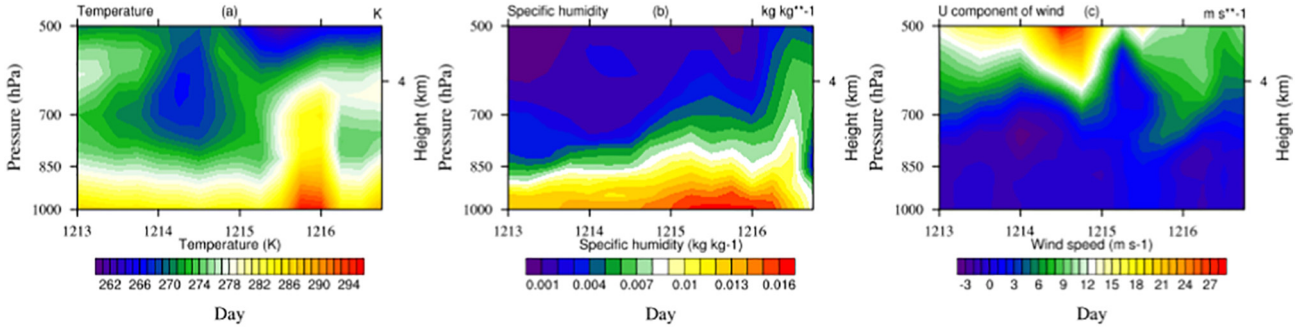

Fig. 3. Variation of (a) temperature (units: K), (b) specific humidity (units: kg kg^{-1}) and (c) horizontal wind speed (units: m s^{-1}) with time at Chengdu station using the ERA-Interim reanalysis dataset from December13 to December 16, 2017. Time is UTC with four records on each day.

provided the surface meteorological elements, including the wind speed, temperature and cloudiness.

2.3. Air quality data

Haze pollution occurs more frequently in winter (Ning et al., 2018) and we therefore studied the influence of the BLH on air quality in this season. 95 and 18 stations were used to observe $PM_{2.5}$ (i.e. particles smaller than 2.5 μm) mass concentrations in Sichuan Province and Chongqing city. The $PM_{2.5}$ mass concentrations from December 2014 to February 2019 were obtained from the China Air Quality Online Monitoring and Analysis Platform and were used to study the change in $PM_{2.5}$ characteristics and to investigate the relationship between air pollution and weather conditions. The data available from each station during the observation period were different as a result of the rapid development of the observation networks. The 113 stations were divided into 22 cities to compare air quality in different regions.

2.4. Methods

The total cloud fraction observed at Chengdu and Chongqing meteorological stations was used to divide the observations into clear and cloudy days. A sunny day was defined as when the total cloud fraction during the daytime was <30%; otherwise, the day was defined as cloudy (CMA, 2017). There were about 70 sunny days during the five winters of the study period.

To compare the observations and the value in the ERA-interim, the root-mean-square-error (RMSE) is used, which is defined as

$$\mathrm{RMSE} = \left[M^{-1}\sum\left(f^{ob}-f\right)^2\right]^{1/2} \tag{8}$$

where the summation is made for M observations and f^{ob} and f are the observations and the results of the ERA-interim, respectively.

To evaluate the correlation relationship between surface sensible heat flux or turbulent shear stress and the maximum boundary layer height (h_{max}), a correlation coefficient, denoted R^2, is adopted,

$$R^2(X,Y) = \frac{\mathrm{Cov}^2(X,Y)}{\mathrm{Var}[X]\mathrm{Var}[Y]} \tag{9}$$

where Cov(X, Y) is the covariance between X and Y, Var[X] is the variance of X, Var[Y] is the variance of Y. X is the surface sensible heat flux or the turbulent shear stress, and Y is the maximum boundary layer height (h_{max}).

3. Results and discussion

3.1. Verification of the ERA-interim reanalysis dataset

Fig. S1 compares the temperature profiles of the ERA-Interim and radiosonde datasets at Chengdu and Chongqing stations on cloudy and sunny days. The air temperature from the ERA-Interim dataset agrees well with the observations. There is a slight difference between the ERA-Interim and observational data above a height of 800 hPa, but they reflect the same trend. There is a temperature inversion between 650 and 500 hPa in both datasets. The height of the temperature inversion on cloudy days (Fig. S1a) is lower than that on sunny days (Fig. S1b) in both datasets.

Table 1 gives the root-mean-square errors (RMSEs) between the ERA-Interim dataset and the radiosonde observations at different heights over the five winters. The ERA-Interim data were close to the observational temperature, wind speed and specific humidity and the RMSEs increased with height.

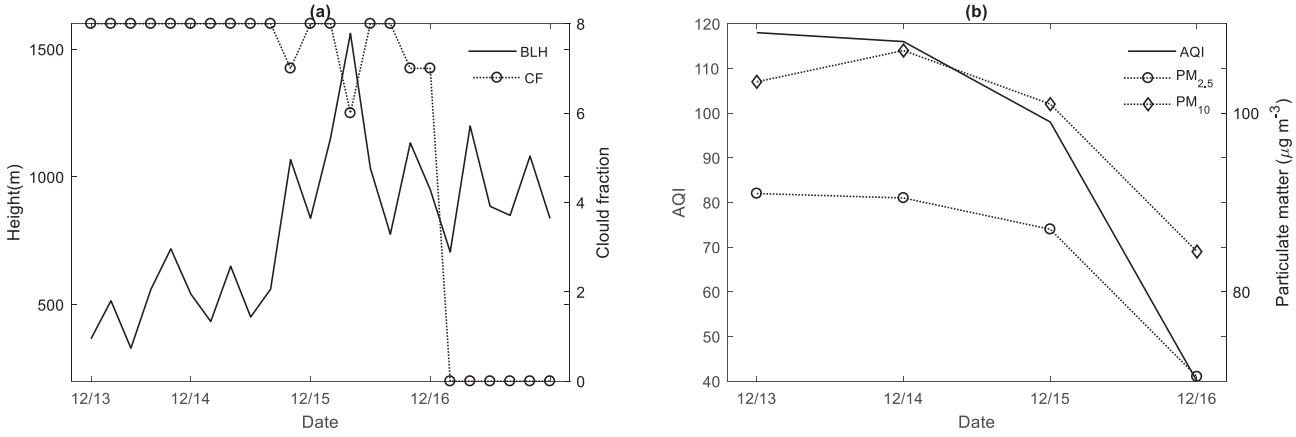

Fig. 4. Variation of (a) the boundary layer height and cloud fraction and (b) $PM_{2.5}$ and PM_{10} and the air quality index with time at Chengdu station from December13 to December 16, 2017.

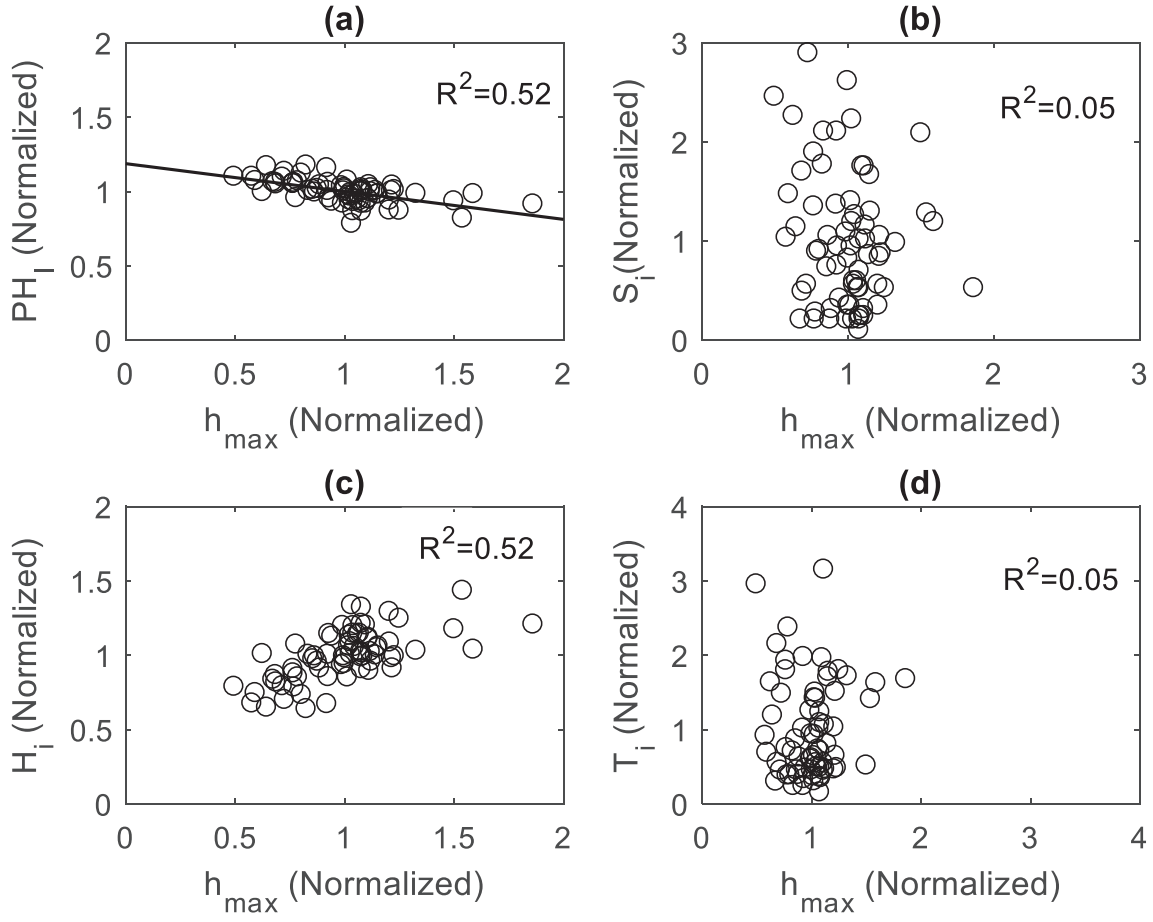

Fig. 5. Relation between the height of the base of the inversion layer and (a) the pressure at the base of the temperature inversion layer (PH_i) and (c) the height of the base of the temperature inversion layer (H_i), (b) the inversion temperature (S_i) and (d) the thickness of the inversion layer (T_i) and the boundary layer height on cloudy days.

The comparison of seasonally averaged BLHs derived from observations and ERA-interim reanalysis shows good agreement on average (Guo et al., 2016). In addition, the BLH, is difficult to be derived from soundings in the case of a weak inversion or a non-perfectly mixed boundary layer, and at the time when the stable boundary layer turn to the convective boundary layer (Seidel et al., 2010). Furthermore, the radiosonde humidity sensor can introduce systematic errors in clod and dry or cloudy conditions (Seidel et al., 2012) which originate from changes in instruments, observational practices, processing procedures, station relocations, and other issues, resulting in many spurious changes and discontinuities (Wang and Wang, 2014). Therefore, the ERA-Interim dataset was suitable for use in our analyses. The focus of our study was the daily maximum BLH (h_{max}), which represents the final status of the CBL.

3.2. Influence of clouds and the inversion layer on h_{max}

Fig. 2 shows the distribution of h_{max} in the Sichuan Basin on sunny (Fig. 2a) and cloudy (Fig. 2b) days during the winter from 2014 to 2019; h_{max} was higher on sunny days than on cloudy days.

Fig. 3 shows the evolution of temperature, the water vapor mixing ratio and the horizontal wind speed profiles during the transitional period from December 13 to 16, 2017. December 13–14 were cloudy days and December 15–16 were sunny days. There was an inversion layer from 700 to 500 hPa on December 13–14, 2017. Jiang et al. (2009) suggested that an inversion layer at this height is formed by the uplift of surface heat from the Qinghai–Tibetan Plateau and a prevailing westerly wind in winter. The inversion layer disappeared during the following day (December 15, 2017).

Table 2
Monthly distribution of elements on sunny and cloudy days at Chengdu.

Year	Sunny days						Cloudy days					
	AQI	h_{max} (m)	SSHF (W m^{-2})	W_{sh} (N m^{-2} s)	PH_i (hPa)	H_i (m)	AQI	h_{max} (m)	SSHF (W m^{-2})	W_{sh} (N m^{-2} s)	PH_i (hPa)	H_i (m)
Y1	105	980	169	1812	644	3746	205	908	160	1699	673	3230
Y2	111	912	130	1993	664	3419	204	892	127	1670	708	2962
Y3	88	1228	303	4931	638	3770	172	1111	289	4484	680	3284
Y4	90	1254	326	4643	604	3749	181	1123	238	4390	623	3123
Y5	72	1378	389	4682	613	3770	172	1213	289	4362	664	3320

AQI, air quality index; SSHF, surface sensible heat flux; W_{sh}, turbulent shear stress.

Table 3
Monthly distributions of elements on sunny and cloudy days at Chongqing.

Year	Sunny days						Cloudy days					
	AQI	h_{max} (m)	SSHF (W m^{-2})	W_{sh} (N m^{-2} s)	PH_i (hPa)	H_i (m)	AQI	h_{max} (m)	SSHF (W m^{-2})	W_{sh} (N m^{-2} s)	PH_i (hPa)	H_i (m)
Y1	118	951	178	1778	636	3920	241	908	143	1621	645	3348
Y2	124	936	142	1854	612	3365	229	892	136	1751	726	2864
Y3	98	1466	318	4459	659	3425	198	1335	245	4189	691	3248
Y4	105	1342	320	4642	641	3558	152	1284	271	4126	683	3367
Y5	122	1568	334	4581	626	3565	134	1356	236	4184	657	3369

Fig. 3b shows that there was an inversion layer in the specific humidity between 700 and 500 hPa on December 13, 2017, which disappeared on December 15–16. The isohumidity line changed steadily with time. Fig. 4c shows the variation in wind speed with time. The wind speed between 1000 and 850 hPa was low on December 13–14 and the distribution of isovelocity line was sparse. The wind speed increased on December 15–16 and the distribution of isovelocity line became dense. The inversion temperature disappeared, the water vapor content decreased, the wind speed increased and h_{max} increased when the cloudy days changed to sunny days, in contrast with the results reported by Jiang et al. (2009) and Ning et al. (2018). The inversion temperature therefore may not be the main factor affecting h_{max} on sunny days.

Fig. 4a shows the relationship between the cloud fraction and h_{max}. The cloud fraction on December 13–14 was 8 and h_{max} gradually increased from December 13 to 16. The formation of this type of cloud is related to the inversion layer in the lower troposphere (J. Li et al., 2016). The cloud fraction gradually decreased to 0 from December 14 to 16, indicating that the cloudy days changed to sunny days. Fig. 4b shows the changes in $PM_{2.5}$, PM_{10} (i.e. particles smaller than 10 μm) and the air quality index over time. The air quality index decreased from 115 on December 13 to 40 on December 16, the concentration of PM_{10} decreased from 105 μg m^{-3} on December 13 to 70 μg m^{-3} on December 16, and the concentration of $PM_{2.5}$ decreased from 80 μg m^{-3} on December 13 to 40 μg m^{-3} on December 16, indicating that the concentration of pollutants decreased and the air quality improved. Therefore when cloudy days turned to sunny days, the inversion temperature disappeared and there was a decrease in the water vapor content and cloud fraction, although h_{max} increased. These results led to a decrease in the concentration of pollutants.

To analyze further the effect of the temperature inversion on h_{max}, we selected all the cloudy days from the 2014–2019 winters and then investigated the relationship between the height of the base of the temperature inversion layer (H_i), the pressure at the base of the temperature inversion layer (PH_i), the size of the temperature inversion (S_i), the thickness of the inversion layer (T_i) and h_{max} (Fig. 5). All the data series were normalized to facilitate the comparison, which was obtained using the average value. There was a strong correlation between PH_i (H_i) and h_{max} with a correlation coefficient ($R^2 = 0.5$) of 0.5, which passed the salience test at the 95% confidence level. The correlation between S_i and h_{max} was lower than that of PH_i. There was a large gap between the height of the BLH and the height of the inversion layer, which cannot be categorized as the atmospheric boundary layer. The existence of the inversion layer significantly altered the stratification of the atmosphere and affected the distribution of water vapor in the atmosphere. A large amount of water vapor accumulated in the lower troposphere and reached very high levels, contributing to the formation of mid-level clouds in this region.

To further verify the accuracy of these results, we classified the days into cloudy and sunny days (Figs. S2 and S3). We can see that the $PM_{2.5}$, maximum of boundary layer height (h_{max}), surface sensible heat flux (SSHF) and turbulent shear stress (W_{sh}) in sunny day is smaller than that in the cloudy day at Chengdu. During the sunny day, the $PM_{2.5}$ decreases, but the h_{max}, SSHF and W_{sh} increase (Fig. S2a). The results at Chengdu are similar with that in Chongqing (Fig. S3).

They are also classified by year (Tables 2 and 3). In the statistic results, there was little difference between the sunny and cloudy days in different years, but the air quality index on cloudy days was larger than that on sunny days, whereas PH_i and the BLH on cloudy days were lower than those on sunny days, further confirming the accuracy of the statistical results. The inversion layer acted like a cover and h_{max} decreased with an increase in the thickness of the cover, which was not conducive to the diffusion of pollutants. h_{max} increased as the

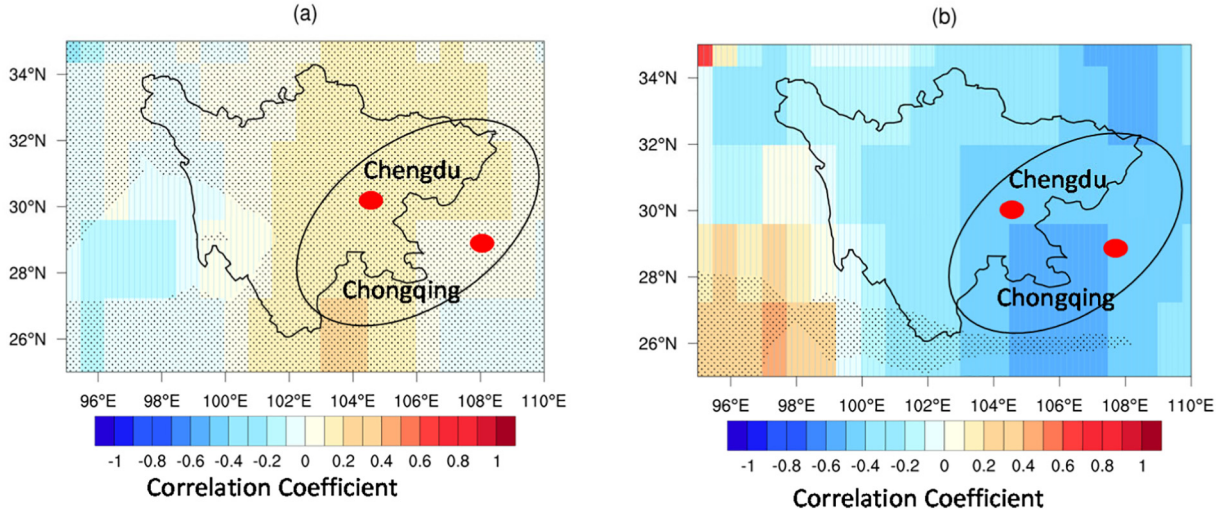

Fig. 6. Significance test of the correlation between the sensible heat flux and the maximum of the boundary layer height (h_{max}) on (a) sunny and (b) cloudy days in Sichuan Province. The leftmost red dot is Chengdu and the rightmost red dot is Chongqing. The oval shape reflects the outline of the Sichuan Basin.

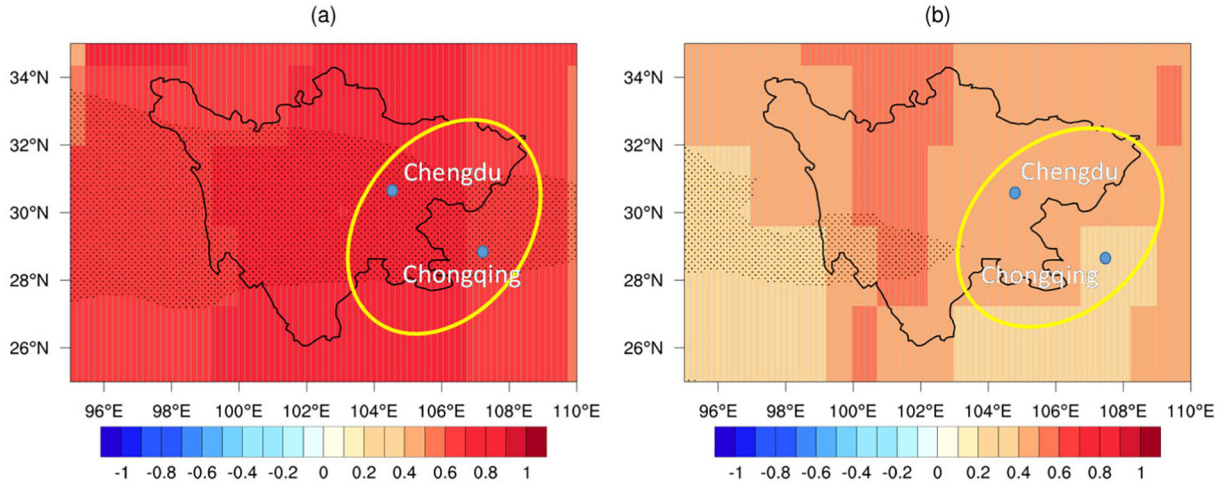

Fig. 7. Significance test of correlation between the wind shear and the boundary layer height on (a) cloudy and (b) sunny days in Sichuan Province. The oval shape reflects the outline of the Sichuan Basin.

thickness of the cover decreased, which favored the dispersion of pollutants. The results for Chongqing city were similar to those for Chengdu, consistent with the results of Ning et al. (2018).

3.3. Influence of the sensible heat flux on h_{max}

Our study of the effect of the inversion layer showed that it is necessary to determine the other factors that affect h_{max} on sunny days. We therefore investigated the influence of the sensible heat flux on h_{max}. Fig. 6 shows the results of the significance test for the correlation between the sensible heat flux and h_{max} on both cloudy (Fig. 6a) and sunny (Fig. 6b) days in the Sichuan Basin during the study period. There was a good correlation between h_{max} and the sensible heat flux in the central Sichuan Basin on sunny days (shaded area) with a confidence level >95%. By contrast, the correlation between h_{max} and the sensible heat flux over the Qinghai–Tibetan Plateau in western Sichuan was

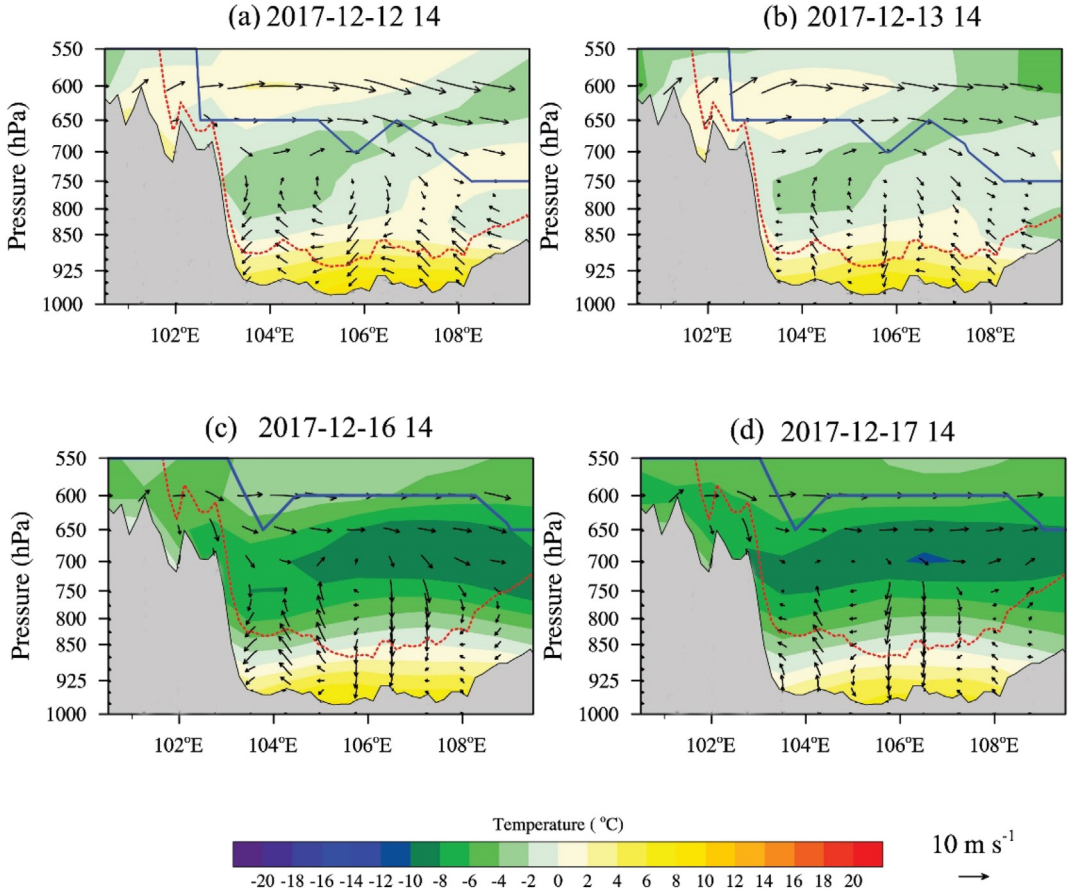

Fig. 8. West–east vertical cross-sections of temperature (shading; units: °C) and wind vectors (synthesized by u and w) through the Sichuan Basin (30.75° N) on sunny days at (a) 14:00 BST on December 12, 2019, (b) 08:00 BST on December 13, 2017 and on cloudy days at (c) 14:00 BST on December 16, 2017 and (d) 14:00 BST on December 17, 2017. The vertical velocity is multiplied by 100 when plotting the wind vectors. The gray shading represents the terrain. The solid line represents the base of the inversion layer and the red dotted line represents h_{max}.

not significant at the 5% level. The significance tests showed that the sensible heat flux was not an important factor in determining h_{max} on cloudy days, which further confirms that the main factor influencing h_{max} on cloudy days was the inversion layer.

Based on the spatial correlation between the sensible heat flux and h_{max} in the Sichuan Basin, we selected sites in different regions and at Chengdu and Chongqing (Fig. S4) stations for further investigation. The results showed a clear linear correlation between the sensible heat flux and h_{max} on sunny days at Chengdu and Chongqing (Fig. S4a) that was larger than the correlation on cloudy days (Fig. S4b). The value of h_{max} increased with the increase in the sensible heat flux, indicating that the relationship between h_{max} and the sensible heat flux was better than that on cloudy days.

3.4. Influence of wind shear on h_{max}

Fig. 7 shows the significance test for the correlation between the turbulent surface stress and h_{max} on both sunny (Fig. 7a) and cloudy (Fig. 7b) days in the Sichuan Basin during the study period. The turbulent surface stress can be used to represent the wind shear. The correlation between h_{max} and the turbulent surface stress in the central region of the Sichuan Basin was excellent on sunny days, with a correlation coefficient close to 1, and passed the significance test at the 5% level. The value of h_{max} increased with an increase in the turbulent surface stress, indicating that this made a profound contribution to the boundary layer. By contrast, the relationship between h_{max} and the turbulent surface stress passed the significance test in only a few regions on cloudy days, indicating that the turbulent surface stress was not an important factor in determining h_{max} on cloudy days. This result further confirms that the inversion layer is the main factor affecting h_{max} on cloudy days.

Chengdu was selected as a representative station to further study the relationship between wind shear (turbulent surface stress) and h_{max} (Fig. S5). The correlation between h_{max} and wind shear was very good on sunny days. The correlation coefficient was almost 1, and was significant at the 5% level in sunny days. The correlation coefficient was only 0.1 and was not significant at the 5% level in cloudy days. The results at Chengdu were similar to those at Chongqing. The value of h_{max} increased with an increase in the turbulent surface stress, indicating that the turbulent surface stress made a key contribution to the BLH.

3.5. Effect of terrain on h_{max}

Fig. 8 shows west–east vertical cross-sections of the temperature and wind vectors (synthesized by u and w) through the Sichuan Basin during both sunny and cloudy days to explain why h_{max} was closely related to the wind shear. Fig. 8a shows that there was a temperature inversion at 650 hPa height on cloudy days and that a secondary circulation occurred in the basin. Fig. 8c shows that the inversion layer formed above 600 hPa on sunny days, higher than on cloudy days. There was a normal vertical lapse rate at 750–700 hPa on cloudy days (Fig. 8c). The secondary circulation was stronger than that on cloudy days in the Sichuan Basin. The wind direction in Chengdu was from the top to the bottom of the mountains.

The value of h_{max} was higher on sunny days than on cloudy days as a result of the mechanical turbulence induced by the terrain. The secondary circulation in the boundary layer was stronger on sunny days than on cloudy days. This secondary circulation was induced by the terrain and was similar to a mountain valley breeze. This stronger secondary circulation increased the wind shear and turbulent mixing and provided the energy required to increase h_{max}, resulting in the transport of pollutants between the city and the mountains, increasing pollution (Huang et al., 2018). This is the reason why the wind shear makes a major contribution to the increase in h_{max} on sunny days.

4. Conclusion

We used observational and reanalysis data for the winter months of 2014–2019 to investigate the effect of the BLH on both cloudy and sunny days and the relationship between the BLH and air quality.

Our results show that the inversion layer in the lower troposphere has a vital impact on the BLH on cloudy days. While on sunny days, the inversion layer disappears as the amount of water vapor and cloud fraction decrease and h_{max} increases. The sensible heat flux and wind shear are the main influencing factors on sunny days, although the contribution of the sensible heat flux is less than that of the wind shear. This is largely due to the turbulence is mainly caused by mechanical mixing of the secondary circulation. The secondary circulation induced by the topographic effects of the Tibetan Plateau is weaker on cloudy days than on sunny days.

Declaration of competing interest

We declare that we have no financial and personal relationships with other people or organizations that can inappropriately influence our work. There is no professional or other personal interest of any nature or kind in any product, service and/or company that could be construed as influencing the position presented in, or the review of, the manuscript entitled.

Acknowledgments

The air quality observation data in this study were supplied by the China Air Quality Online Monitoring and Analysis Platform (www.aqistudy.cn/historydata/?Tdsourcetag=s_pcq_aiomsg). The meteorological observational data were provided by Chengdu and Chongqing stations. This work was funded by the National Key Research and Development Program of China (2018YFC0214002, 2018YFC1505702), National Natural Science Foundation of China (91644226), Project of Science and Technology Plan of Sichuan (2018JY0011, 2019YJ0408), the Desert Meteorological Science Research Fund of China (Sqj2018006) and Chengdu University of Information Technology of Foundation (KYTZ201810).

Appendix A. Supplementary data

Supplementary data to this article can be found online at https://doi.org/10.1016/j.scitotenv.2020.138584.

References

Beljaars, A., 2006. Chapter 3: turbulent transport and interactions with the surface. Part IV: Physical Processes, IFS Documentation, Operational Implementation 12 September 2006 Cy31r1 31, ECMWF, Shinfield Park, Reading, RG2 9AX, England.

Bi, J., Huang, J., Hu, Z., Holben, B.N., Guo, Z., 2014. Investigating the aerosol optical and radiative characteristics of heavy haze episodes in Beijing during January of 2013. J. Geophys. Res. Atmos. 119 (16), 9884–9900. https://doi.org/10.1002/2014JD021757.

Cai, W., Li, K., Liao, H., et al., 2017. Weather conditions conducive to Beijing severe haze more frequent under climate change. Nat. Clim. Chang. 7 (4), 257–262.

Chen, H., Wang, H., 2015. Haze days in North China and the associated atmospheric circulations based on daily visibility data from 1960 to 2012. J. Geophys. Res. Atmos. 120 (12), 5895–5909.

CMA, 2017. Basic Terminology of Weather Forecast. Standards Press of China, Beijing.

Cohen, A.J., Brauer, M., Burnett, R., et al., 2017. Estimates and 25-year trends of the global burden of disease attributable to ambient air pollution: an analysis of data from the Global Burden of Diseases Study 2015. Lancet 389 (10082), 1907–1918.

Deng, T., Wu, D., Deng, X., Tan, H., Li, F., Liao, B., 2014. A vertical sounding of severe haze process in Guangzhou area. Sci. China Earth Sci. 57, 2650–2656. https://doi.org/10.1007/s11430-014- 4928-y.

Gu, Y., Yim, S.H.L., 2016. The air quality and health impacts of domestic trans-boundary pollution in various regions of China. Environ. Int. 97, 117–124. https://doi.org/10.1016/j.envint.2016.08.004.

Guo, J., Miao, Y., Zhang, Y., et al., 2016. The climatology of planetary boundary layer radiosonde and reanalysis data. Atmos. Chem. Phys. 16 (20), 13309–13319.

Han, B., Zhao, C., Lv, S., et al., 2015. A diagnostic analysis on the effect of the residual layer in convective boundary layer development near Mongolia using 20th century reanalysis data. Adv. Atmos. Sci. 32 (6), 807–820.

Huang, Q., Wang, R., Tian, W., et al., 2014. Study of the impacts of wind shear on boundary layer convection based on the large eddy simulation. Acta Meteor. Sinica 72 (1), 100–115. https://doi.org/10.11676/qxxb2014.007 (in Chinese).

Huang, Xiaojuan, Zhang, Junke, Luo, Bin, Wang, Lili, Tang, Guiquan, Liu, Zirui, Song, Hongyi, Zhang, Wei, Yuan, Liang, Wang, Yuesi, 2018. Water-soluble ions in $PM_{2.5}$ during spring haze and dust periods in Chengdu, China: Variations, nitrate formation and potential source areas. Environ. Pollut. 243, 1740–1749. https://doi.org/10.1016/j.envpol.2018.09.126.

Jiang, X., Li, Y., Wang, X., et al., 2009. The observational analysis of atmospheric boundary layer structure in east part and downstream of Tibetan Plateau. Plateau Meteorol. 754–762 (in Chinese).

Künzli, N., Jerrett, M., Mack, W.J., et al., 2005. Ambient air pollution and atherosclerosis in Los Angeles. Environ. Health Perspect. 113 (2), 201–206.

LeMone, M.A., Chen, F., Alfieri, J.G., et al., 2007. Influence of land cover and soil moisture on the horizontal distribution of sensible and latent heat fluxes in Southeast Kansas during IHOP_2002 and CASES-97. J. Hydrometeorol. 8 (1), 68–87. https://doi.org/10.1175/JHM554.1.

Li, J., Li, C., Zhao, C., et al., 2016a. Changes in surface aerosol extinction trends over China during 1980–2013 inferred from quality-controlled visibility data. Geophys. Res. Lett. 43, 8713–8719.

Li, Q., Zhang, R., Wang, Y., 2016b. Interannual variation of the wintertime fog-haze days across central and eastern China and its relation with East Asian winter monsoon. Int. J. Climatol. 36 (1), 346–354.

Liao, T., Wang, S., Ai, J., et al., 2017. Heavy pollution episodes, transport pathways and potential sources of PM2.5 during the winter of 2013 in Chengdu (China). Sci. Total Environ. 584-585, 1056–1065.

Liao, T., Gui, K., Jiang, W., et al., 2018. Air stagnation and its impact on air quality during winter in Sichuan and Chongqing, southwestern China. Sci. Total Environ. 635, 576.

Maronga, B., Raasch, S., 2013. Large-eddy simulations of surface heterogeneity effects on the convective boundary layer during the LITFASS-2003 experiment. Bound.-Layer Meteor. 146, 17–44.

Moeng, C.H., Sullivan, P.P., 1994. A comparison of shear-driven and buoyancy-driven planetary boundary-layer flows. J. Atmos. Sci. 51, 999–1022.

Ning, G., Wang, S., Ma, M., et al., 2017. Characteristics of air pollution in different zones of Sichuan Basin, China. Sci. Total Environ. 612, 975–984.

Ning, G., Wang, S., Yim, S.H.L., et al., 2018. Impact of low-pressure systems on winter heavy air pollution in the Northwest Sichuan Basin, China. Atmos. Chem. Phys. 18 (18), 13601–13615.

Ning, G., Yim, S.H.L., Wang, S., et al., 2019. Synergistic effects of synoptic weather patterns and topography on air quality: a case of the Sichuan Basin of China. Clim. Dyn. 53 (11), 6729–6744.

Pope, C.A., Burnett, R.T., Thun, et al., 2002. Lung cancer, cardiopulmonary mortality, and long-term exposure to fine particulate air pollution. J. Am. Med. Assoc. 287 (9), 1132–1141.

Seidel, D.J., Ao, C.O., Li, K., 2010. Estimating climatological planetary boundary layer heights from radiosonde observations: comparison of methods and uncertainty analysis. J. Geophys. Res. 115, D16113. https://doi.org/10.1029/2009JD013680.

Seidel, D.J., Zhang, Y., Beljaars, A., Golaz, J.C., Jacobson, A.R., Medeiros, B., 2012. Climatology of the planetary boundary layer over the continental United States and Europe. J. Geophys. Res. 117, D17106. https://doi.org/10.1029/2012JD018143.

Sheehan, P., Cheng, E., English, A., et al., 2014. China's response to the air pollution shock. Nat. Clim. Chang. 4 (5), 306–309.

Troen, I.B., Mahrt, L., 1986. A simple model of the atmospheric boundary layer; sensitivity to surface evaporation. Bound.-Layer Meteorol. 37 (1–2), 129–148.

Wang, X., Wang, K., 2014. Estimation of atmospheric mixing layer height from radiosonde data. Atmos. Meas. Tech. 7 (6), 1701–1709.

Wang, X., Wang, K., Su, L., 2016. Contribution of atmospheric diffusion conditions to the recent improvement in air quality in China. Sci. Rep. 6, 36404.

Ye, X., Song, Y., Cai, X., Zhang, H., 2016. Study on the synoptic flow patterns and boundary layer process of the severe haze events over the North China Plain in January 2013. Atmos. Environ. 124, 129–145. https://doi.org/10.1016/j.atmosenv.2015.06.011.

Zhang, Y.L., Cao, F., 2015. Fine particulate matter (PM2.5) in China at a city level. Sci. Rep. 5, 14884.

Zhang, G.Z., Xu, X.D., Wang, J.Z., 2003. A dynamic study of Ekman characteristics by using 1998 SCSMEX and TIPEX boundary layer data. Adv. Atmos. Sci. 20 (3), 349–356.

Zhang, R.H., Li, Q., Zhang, R.N., 2014. Meteorological conditions for the persistent severe fog and haze event over eastern China in January 2013. Sci. China Earth Sci. 57 (1), 26–35.

Zhang, Z., Zhang, X., Gong, D., Kim, S.-J., Mao, R., Zhao, X., 2016. Possible influence of atmospheric circulations on winter haze pollution in the Beijing–Tianjin–Hebei region, northern China. Atmos. Chem. Phys. 16, 561–571. https://doi.org/10.5194/acp- 16-561-2016.